Behavior of reinforced concrete stair slabs strengthened with steel plates and near surface mounted steel bars

Engineering Structures 292 (2023) 116514

Contents lists available at ScienceDirect

Engineering Structures

journal homepage: www.elsevier.com/locate/engstruct

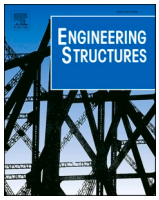

Behavior of reinforced concrete stair slabs strengthened with steel plates and near surface mounted steel bars

Ahmed A. Hamoda [a], Boshra A. Eltaly [b], Rania E. Sera [b], Qing Quan Liang [c,*]

[a] Civil Engineering Dept., Faculty of Engineering, Kafrelsheikh University, Kafrelsheikh, Egypt
[b] Civil Engineering Dept., Faculty of Engineering Menoufia University, Egypt
[c] College of Sport, Health, and Engineering, Victoria University, PO Box 14428, Melbourne, VIC 8001, Australia

ARTICLE INFO

Keywords:
Reinforced concrete stair slabs
Near surface mounted
Steel plates
Strengthening techniques
Finite element modeling

ABSTRACT

The bends in Reinforced Concrete Stair Slabs (RCSS) subjected to opening moments may be damaged due to improper detailing of tensile reinforcement or construction errors. The damaged bends in RCSS need to be strengthened to restore their flexural strengths. However, there are very limited investigations into the behavior of strengthened RCSS. This paper reports experimental and simulation works on the structural behavior of RCSS strengthened with externally bonded steel plates and near surface mounted steel bars. The test program and results of six full-scale strengthened RCSS loaded to failure are described in detail. A finite element model is developed using ABAQUS to simulate the experimentally measured responses of strengthened RCSS. It is shown that the utilized strengthening techniques significantly improve the cracking load, ultimate load, and energy absorption capacity of RCSS. There is a good agreement between computer simulations and experimental results, suggesting that the model of nonlinear inelastic analysis can be used with confidence to conduct further parametric studies.

1. Introduction.

Reinforced concrete stairs are important structural members used as transits in multistory reinforced concrete buildings [1–3]. Many buildings all over the world are counted unsafe because of the requirements of new codes, the changes in building usage, improper design, construction errors, and increased loads [4]. The bends in Reinforced Concrete Stair Slabs (RCSS) under opening moments may be damaged owing to improper detailing of tensile reinforcement in the slabs and construction errors. The damaged bends in RCSS need to be strengthened to restore their load-carrying capacities. However, the behavior of RCSS strengthened by available techniques has not been fully understood due to the lack of experimental and simulation studies. This paper addresses this problem by reporting new test results and computer modeling of RCSS strengthened by innovative techniques.

In recent decades, external strengthening techniques have been used to strengthen structural members in many experimental studies [5–7]. Afefy et al. [8] found that these techniques mainly enhance the strength and ductility of strengthened members. Dong et al. [9] examined experimentally the flexural strengthening of reinforced concrete slabs using textile reinforced mortar enhanced by short PVA fibers. It was found that the strengthening method of using fibers significantly enhances the overall behavior of strengthened slabs as well as their elastic stiffnesses. In this regard, Wang et al. [10] found that increasing the proportion of PVA fibers led to a reduction in the workability of concrete. Zhang et al. [11] investigated experimentally and numerically the flexural behavior of concrete slabs strengthened with textile reinforced geopolymer mortar. The test results showed that textile reinforced geopolymer mortar is an effective strengthening technique for improving the flexural performance and post-cracking stiffness of reinforced concrete slabs.

One of the latest and most promising strengthening techniques for reinforced concrete structures is the Near-Surface Mounted Steel Bars (NSMSB). It can offer an easy and effective option of rehabilitating any part of the structure [12–14]. The method of NSMSB has many advantages over other strengthening techniques, including high strength to weight ratio, ease of installation, availability, and durability [15–18]. Kamonna and Abd Al-Sada [19] studied experimentally the strengthening of RC one-way slabs using NSMSB. It was concluded that the NSMSB could crucially improve the ultimate capacity and energy absorption capacity of the slabs. Rahal and Rumaih [20] undertook tests on the shear behavior of reinforced concrete beams strengthened using

* Corresponding author at: College of Sport, Health, and Engineering, Victoria University, PO Box 14428, Melbourne, VIC 8001, Australia.
E-mail address: Qing.Liang@vu.edu.au (Q.Q. Liang).

https://doi.org/10.1016/j.engstruct.2023.116514
Received 31 January 2023; Received in revised form 26 March 2023; Accepted 19 June 2023
Available online 27 June 2023

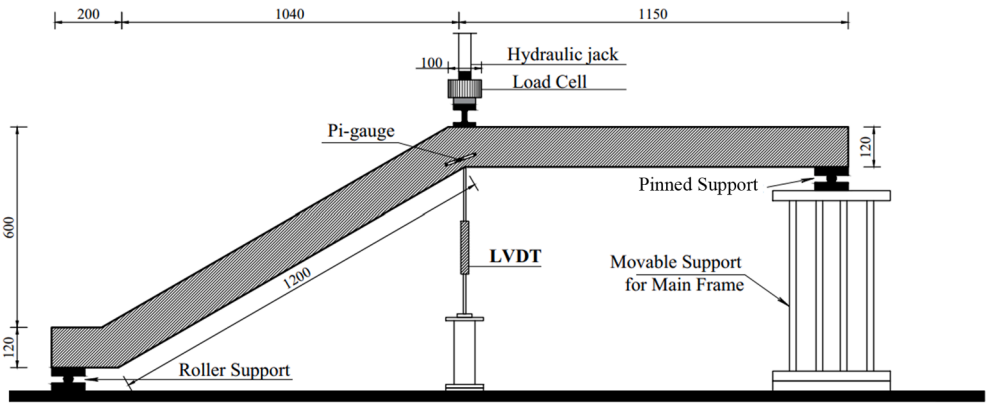

(a)

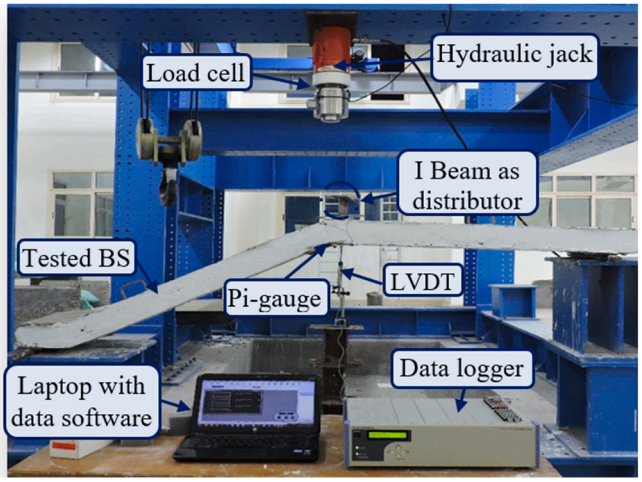

(b)

Fig. 1. Test set-up: (a) schematic illustration; (b) photo.

either NSMSB or Carbon-Fiber-Reinforced Polymers (CFRP). The shear strength was found to considerably increase by bending the steel bars up at 45° with respect to the longitudinal axis of the beam. The use of Near-Surface Mounted CFRP (NSM-CFRP) technique improved the load-carrying capacity of RC beams, but it reduced their ductility [21,22]. Almusallam et al. [23] reported that increasing the ratio of NSMSB or NSM-CFRP increased both the flexural capacity and effective pre-yield stiffness of reinforced concrete beams.

Externally Bonded Steel Plates (EBSP) with adhesive materials have been used to strengthen reinforced concrete members [24]. The epoxy is the most used adhesive material, which requires perfect preparation of concrete surface to remove the external weak layer that may cause poor and inappropriate attachment [25]. Mostofinejad and Kashani [25] reported that the EBSP with a good surface preparation increased about

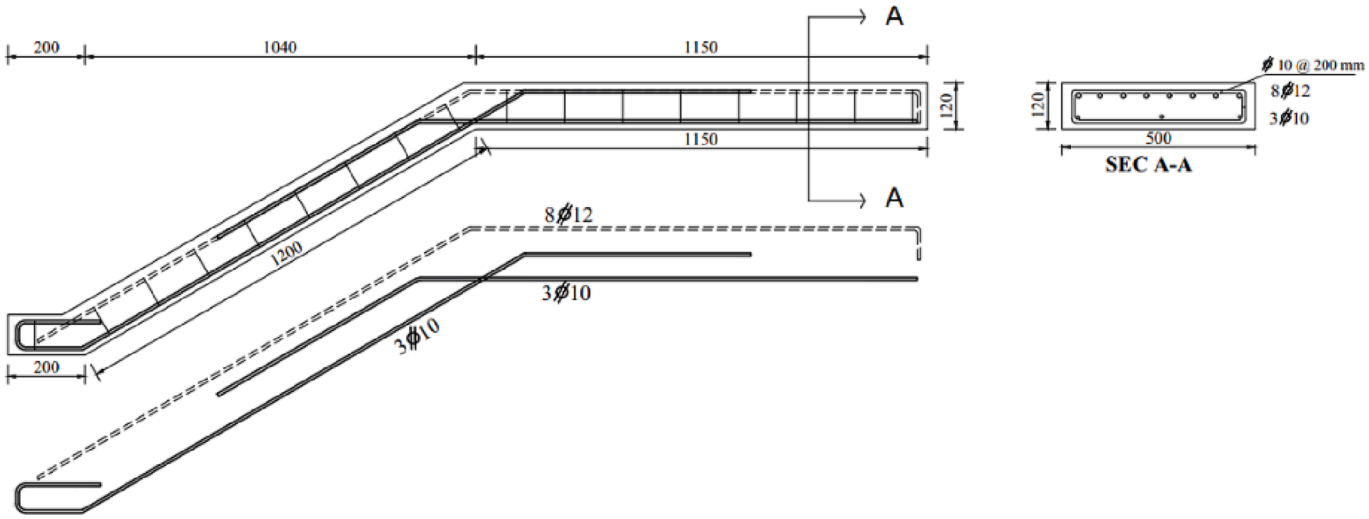

Fig. 2. Dimensions and reinforcement details of stair slab.

Table 1
Test Matrix.

Group	Specimen's ID	Concrete type	Strengthening technique	L_e	Thickness of SPs (or) bar diameter	Note
G1	S-So	NC	EBR with SPs		—	
	S-E-CSPs	NC		200 mm	t_s = 4 mm	Fig. 5(a)
	S-E-LSPs	NC				Fig. 5(b)
G2	S-So	NC		—	—	
	S-N-10D	NC	NSM with steel bars	10D	D = 10 mm	Fig. 5(c)
	S-N-15D	NC		15D		
	S-N-20D	NC		20D		

10–13% the shear strength of the beam compared to that of the one without strengthening. del Rey Castillo et al. [26] found out that the pros of using EBSP system in strengthening are high tensile capacity and better durability to rain and cold weather. However, these advantages can be realized only if the strengthening is properly treated [27–30]. Moreover, the externally bonded techniques have been used with the applications of Fiber-Reinforced Polymer (FRP). Comprehensive investigations have been conducted on the shear and flexural strength as previously reported by [54–56].

Although several studies have been reported on the structural behavior of strengthened reinforced concrete slabs, very limited experiments have been performed on the performance of RCSS strengthened by various techniques. This paper presents experimental and numerical research works on the behavior of RCSS strengthened by using NSMSB and EBSP. The main parameters examined include strengthening technique and type and configuration of reinforcement used for strengthening. A three-dimensional finite element model developed using ABAQUS is described and verified by experimental measurements. Important conclusions drawn from this study are given.

2. Experimental program

2.1. Details of RCSS specimens

The current study focused on examining the performance of strengthened RCSS subjected to flexure induced by a line load applied at the bend as shown in Fig. 1. Six one-way RCSS with identical geometric properties and reinforcement details as shown in Fig. 2 were divided into two groups tabulated in Table 1. The main variables considered were the strengthening techniques, the embedded length (L_e), and configuration of strengthening as shown in Table 1.

Eight deformed steel bars with 12-mm diameter were placed at the top face of the stair slab to prevent compression failure while three 10-mm diameter steel bars were used as tensile reinforcement at the bottom to examine the effect of strengthening techniques. It should be mentioned that the use of lesser tensile reinforcement than compressive one was to prevent the compressive premature failure when adding strengthening reinforcement as previously reported [42,43]. Closed stirrups with 10-mm diameter were used as distributed steel in the transverse direction as shown in Fig. 2. All stair slabs had 500-mm width and 120-mm thickness with a span of 2390 mm. Such geometric details were selected based on previous experimental work [8] and the suitability available for test set-up. The bend in the stair slab had a bending angle of 30° as schematically depicted in Fig. 1(a).

2.2. Material properties and mix proportion

Two different concrete mixes were employed in this investigation: Normal Concrete (NC) and Engineered Cementitious Composite (ECC). The mix proportions for each type can be seen in Table 2. The NC was used to cast all stair slab specimens while ECC was employed as cover concrete to NSMSB as discussed in Section 2.3.

Table 2 provides the average compressive strengths ($f_c^{'}$) of NC and ECC obtained by testing three standard cylinders with dimensions of 150 × 300 mm. The uniaxial tensile test was conducted on NC and the results were utilized in the numerical modeling. The tensile tests on concrete and steel were in accordance with the US specification [31]; the observed modes of failure are presented in Fig. 3. Two different steel bars with diameters of 10 mm and 12 mm were used in this study, which were normal mild steel and high grade one, respectively. The experimental tensile tests for the used steel elements are summarized in Table 3. The measured and idealized stress–strain curves for steels are shown in Fig. 4(a) and Table 3 while the stress–strain relationships for concrete in compression and tension are given in Fig. 4(b). The experimental outcomes showed that the concrete tensile strength was about 2.10 N/mm^2. The bond strength of chemical adhesive epoxy with concrete was 18.4 MPa as reported by Agarwal et al. [57].

2.3. Description of stair slab specimens

The stair slab specimens were divided into two groups depending on the strengthening scenario as shown in Table 1. In Group G1, two of the slabs were strengthened by using EBSP while three of the slabs in Group G2 were strengthened by means of employing NSMSB. As shown in Table 1, the specimens S-So without strengthening were the control ones for comparison purpose. Slab S-E-CSPs was strengthened by longitudinal continuous strips of EBSP. The steel strips were bonded on the bottom surface with chemical epoxy beside anchor bolts to bond strips with concrete at its two ends and mid-span using transverse strip as shown in Fig. 5(a) and Fig. 7. It should be mentioned that the longitudinal steel

Table 2
Mix proportion and concrete compressive strength.

Concrete	Cement (kg/m^3)	Fine aggregate (kg/m^3)	Coarse aggregate (kg/m^3)	Fly ash (kg/m^3)	Water/binder	PVA Fiber (%) in volume	HRWR (kg/m^3)	$f_c^{'}$ (MPa)	Poisson Ratio
NC	350	700	1150	—	0.43	—	—	25	0.2
ECC	550	440	—	600	0.25	2.00	14.5	44	0.22

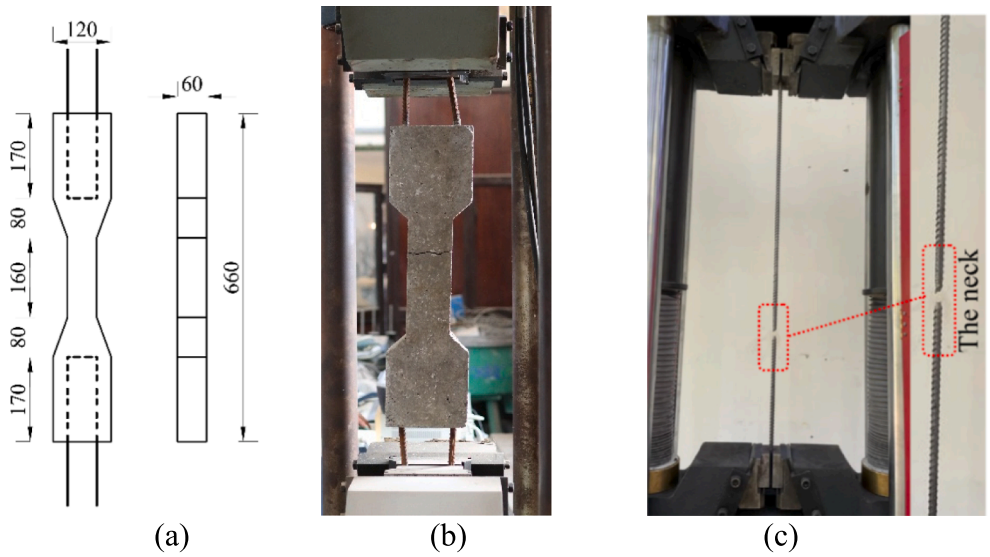

Fig. 3. Material tensile tests: (a) concrete dimensions; (b) test set-up and failure model of NC; (c) tested steel bar.

Table 3
Properties of steel elements.

Material	Yield		Ultimate		Modulus of elasticity (E) (GPa)	Poisson's Ratio
	σ_y (MPa)	ε_y (%)	σ_u (MPa)	ε_u (%)		
Steel bars. #10 mm	296	0.15	565	12.9	197	0.30
Steel bars. #12 mm	404	0.20	674	12.1	202	0.30
Steel Plates.	525	0.256	788	9.4	205	0.30

σ_y = yield stress; ε_y = **y**ield strain; σ_u = ultimate stress; ε_u = **u**ltimate strain.

plates were welded to the transverse steel plate. Slab S-E-LSPs was strengthened with non-continuous strips of EBSP as illustrated in Fig. 5 (b). Similar to the bonding system used for slab S-E-CSPS, the steel strips were bonded on the bottom surface by chemical epoxy and anchor bolts as shown in Fig. 5 (b) and Fig. 7.

The specimens in Group G2 were used to investigate the effectiveness of NSMSB, which were placed longitudinally near the bottom surface as shown in Fig. 5 (c) and Table 1. Three slabs S-N-10D, S-N-15D, and S-N-20D were designed to have embedded lengths of 10D, 15D, and 20D, respectively, where D is the bar diameter as presented in Fig. 5 (c) and Table 1.

2.4. *Casting and strengthening preparation*

Wooden formworks were prepared and used for casting all stair slabs as shown in Fig. 6. The concrete casting was performed in a regular position, which simulated the operation on a construction site. After 28 days, the strengthening process was exploited by placing the slabs in an inverted position so that the bottom of the slab is visible for ease of strengthening as depicted in Figs. 7 and 8. After the tensile surface of the stair slab was roughened, steel plates were externally attached to the surface by using an adhesive chemical epoxy as illustrated in Fig. 7(a). After 24 h epoxy maturity, the longitudinal strips of steel plates were bonded at the ends and critical points in the bend at the bottom surface using embedded bolts as shown in Fig. 7(c).

It is worth mentioning that the preparation of bonding process was not completed in one shot but by separated dependent steps using the type of sandy epoxy which was characterized by hardening without shrinkage. This is because the strengthening technique executed in one shot may result in premature de-bonding during the construction. Firstly, starting from the bend of the RC slab under opening moments, chemical epoxy was added to a part of concrete surface beside filling the

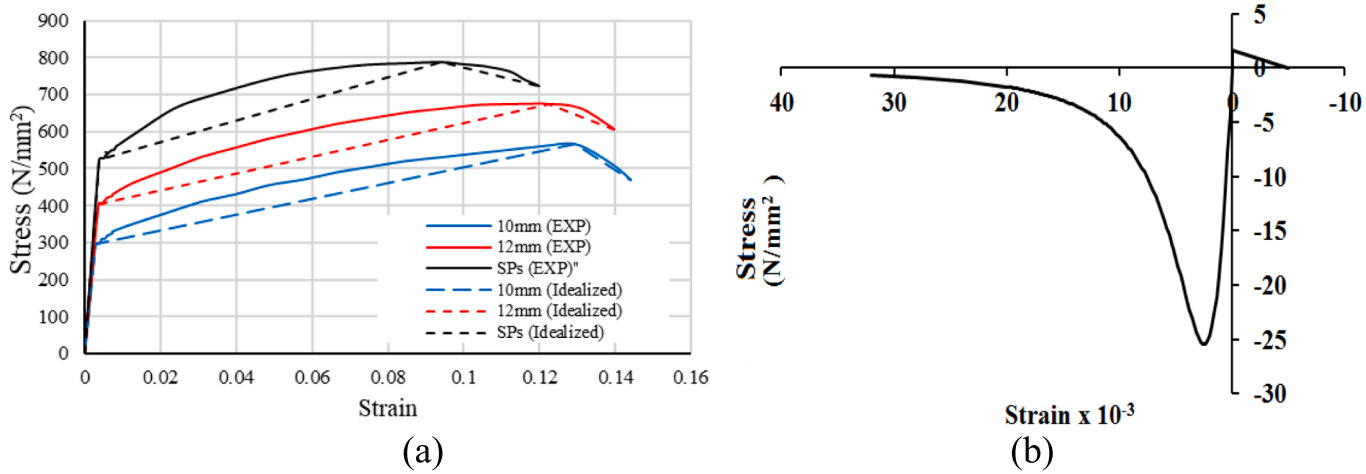

Fig. 4. Stress–strain responses: (a) measured and idealized stress–strain curves for steels; (b) Stress–strain law for NC.

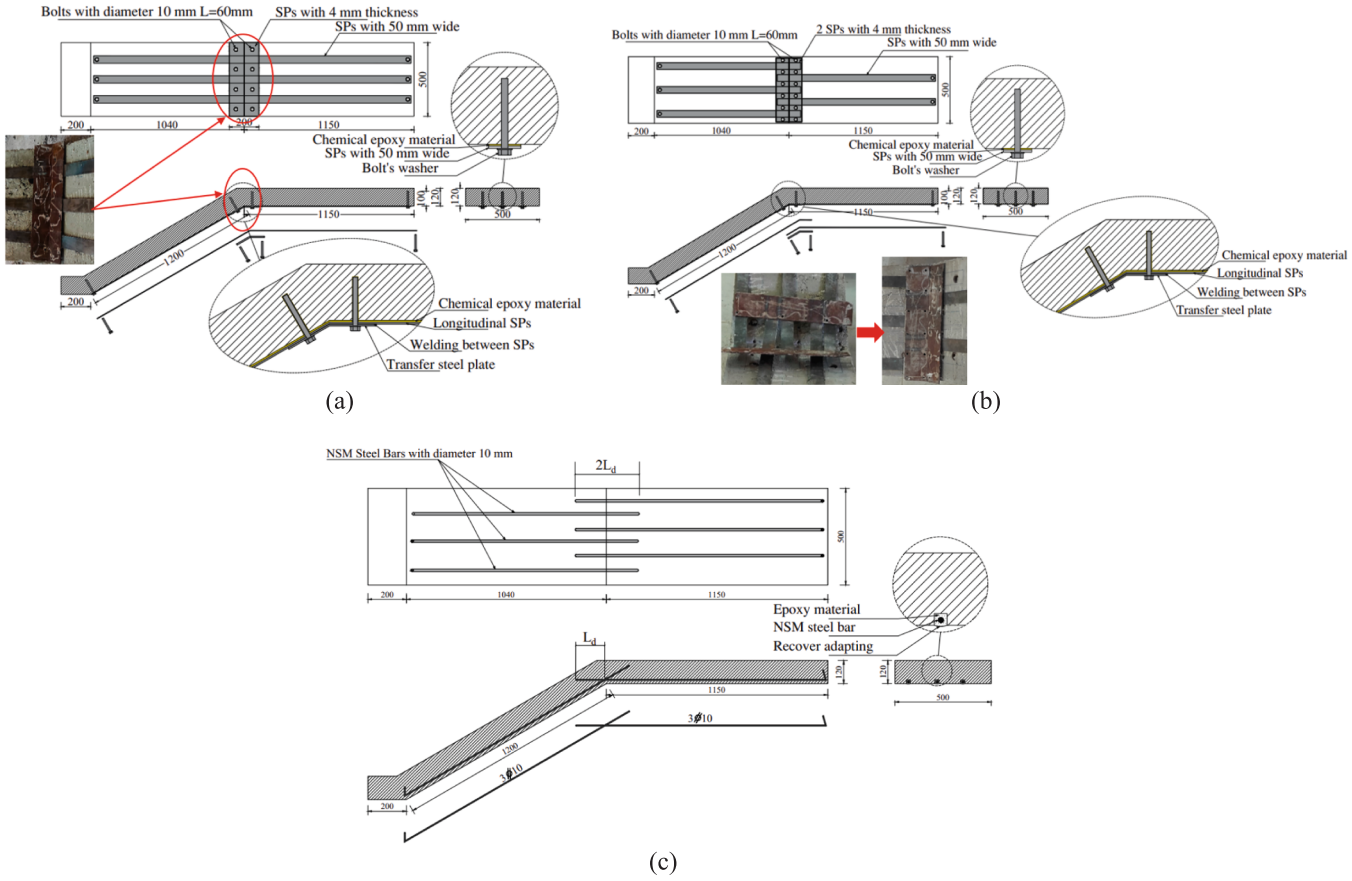

Fig. 5. Geometric details of strengthened stair slabs: (a) Group G1 (S-E-CSPs); (b) Group G1 (S-E-LSPs); (c) Group G2 (strengthening with NSMSB). (Units: mm).

Fig. 6. Formworks and preparation: (a) wooden formworks; (b) during casting process.

perforations of anchor bolts. Then a part of steel strips was fixed to concrete surface from the bend utilizing the bolt‘s washer as shown in Fig. 7. After 24 h, the other parts were bonded by the same steps and utilizing the bolt washers to prevent the de-bonding during construction process.

Fig. 8 presents the preparation of stair slabs strengthened using NSMSB. The strengthening process is summarized as follows: (1) longitudinal grooves with about 20 mm size at the concrete cover was made as illustrated in Fig. 8(a); (2) steel bars with specified embedment lengths were placed in the grooves in bend under opening moments; (3) the epoxy material was used to bond the embedded steel bars; (4) finally, ECC was poured to cover the steel bars as shown in Fig. 8.

2.5. Test setup and instrumentation

Three-dimensional steel frame was constructed and used to carry out the testing of stair slabs as presented in Fig. 1. The stair slab was rested on movable solid steel rods at its ends as roller supports. The vertical line load was applied through the standard I-beam (I.P.N-20) to the specimen by a hydraulic jack of 100 ton-capacity attached to a rigid steel frame as depicted in Fig. 1.

A sensitive load cell was used to record the vertical load as shown in Fig. 1. One Linear Variable Displacement Transducer (LVDT) was positioned at critical/ mid-span point under the tested slab to measure the vertical deflection during the loading process. In addition, electrical pi-gauges having 50-mm gauge length were located at the vertical side of the slab to evaluate and measure the expected flexural cracks. All instrumentations were then connected to Data Acquisition System (DAQ)

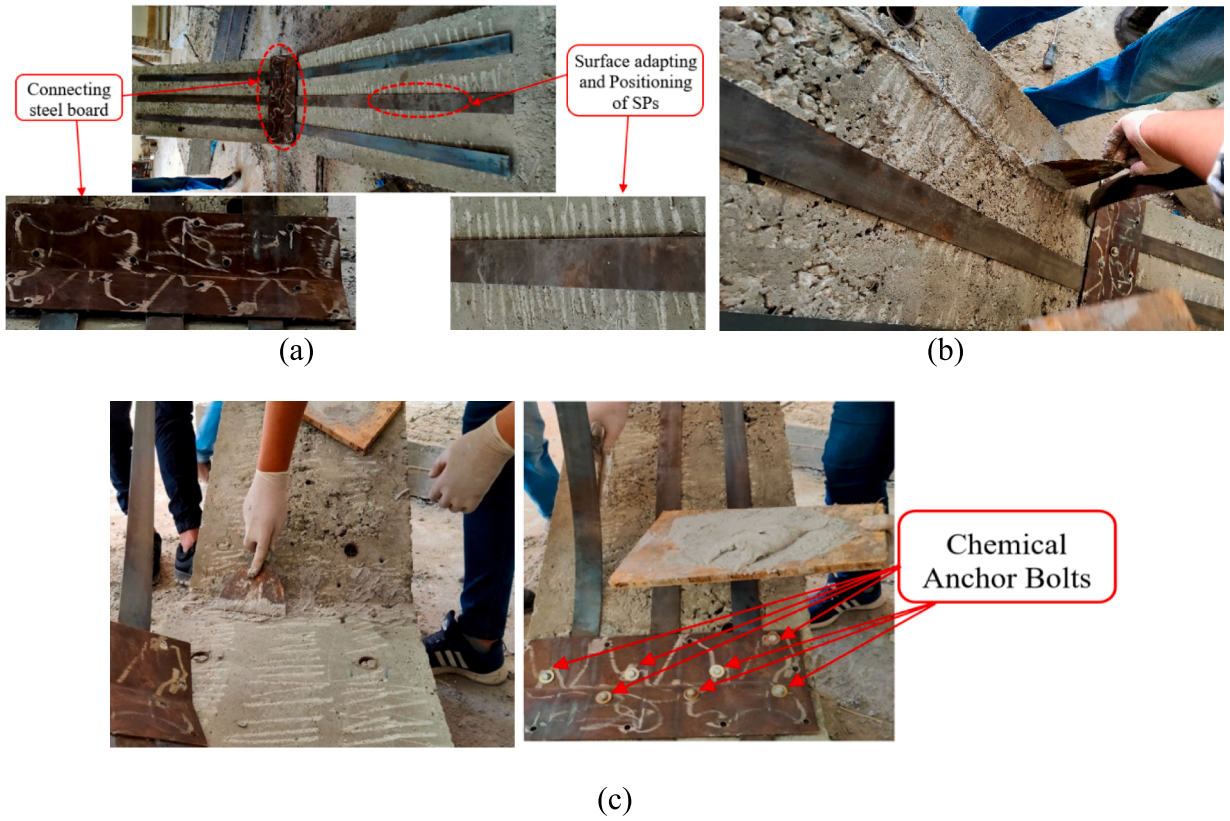

Fig. 7. Strengthening preparation using EBSP for Group G1: (a) surface adapting and positioning of steel plates (SP); (b) bonding of SP; (c) extra bonding by chemical anchor bolts.

Fig. 8. Strengthening preparation using NSMSB for Group G2: (a) surface adapting and installation of steel bars; (b) re-covering of concrete surface by ECC.

to record the readings during the test. The load was applied incrementally. The development and propagation of cracks were marked up to the failure of the tested stair slab.

3. Test results and discussions

3.1. Crack pattern and failure modes

The cracking patterns of all tested stair slabs are presented in Figs. 9-14. Table 4 summarizes all sensitive results obtained from the tests. As shown in Fig. 9, the first visible hair crack in the control specimen S-S0 was detected at the bottom of the bend under opening moments at a load value of 5.70 kN (about 22.0% of P_u). Under the increased load, some similar hair cracks parallel to the first one developed across the bottom surface of the tested stair slab. As the load was increased, the number of such cracks increased, and the cracks extended to the top surface.

The widths of these flexural cracks enlarged with increasing the applied load. Just before failure, the first major crack appeared with wider width, gave the allowance of the tested slab to open with the jacking load. In addition, few longitudinal hair cracks parallel to longitudinal bars initiated at the bottom under the line load as shown on Fig. 9. Finally, the tested slab S-S0 failed suddenly as the flexural bars pulled out of the concrete. The ultimate load of the slab was $P_u = 26$ kN.

The crack patterns of slabs S-E-LSPs and S-E-CSPs are shown in Figs. 10 and 11, respectively. The first hair flexural crack appeared at the bottom zone of the bend in opening moments in the slab S-E-LSPs at $P_{cr} = 13.50$ kN while the cracking load was 15.30 kN for the slab S-E-CSPs as given in Table 4. The initial cracks formed at the bottom of the bend were marked on the side surface since the bottom concrete surface could not be seen due to the existence of steel plates. It can be seen from Table 4 that adding steel plates enhanced the cracking load (P_{cr}) by about 136% and 168%, respectively, compared to that of slab S-S0.

As the load was increased, the cracks extended to the top surface of the tested slab. However, the use of EBSP strengthening techniques

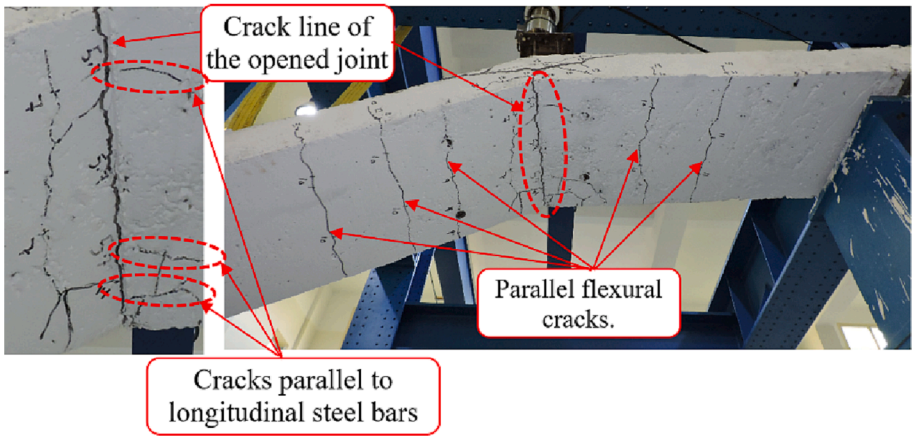

Fig. 9. Crack patterns of the control specimen S-S0.

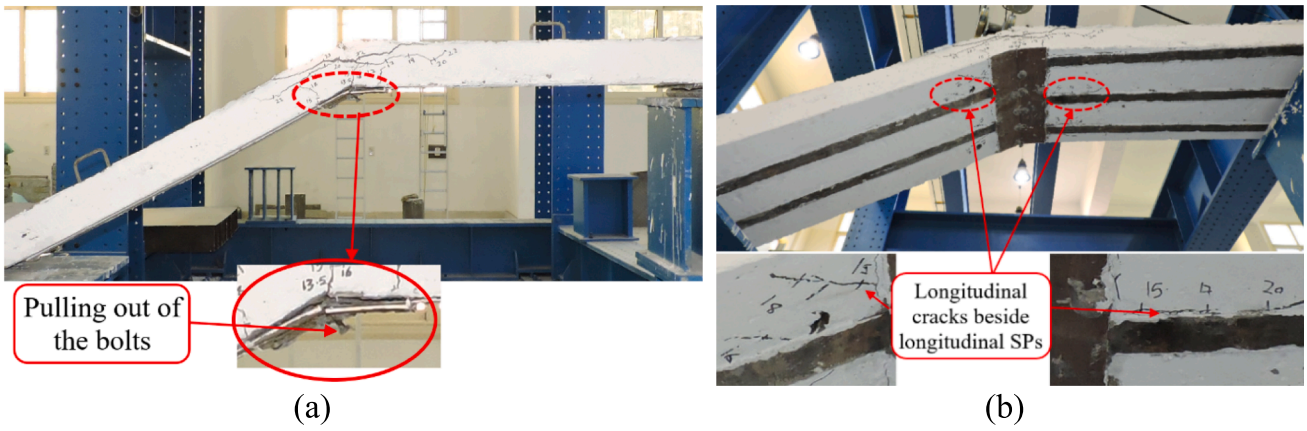

Fig. 10. Crack patterns of slab S-E-LSPs: (a) pulling out of the bolts; (b) cracks parallel to longitudinal steel bars.

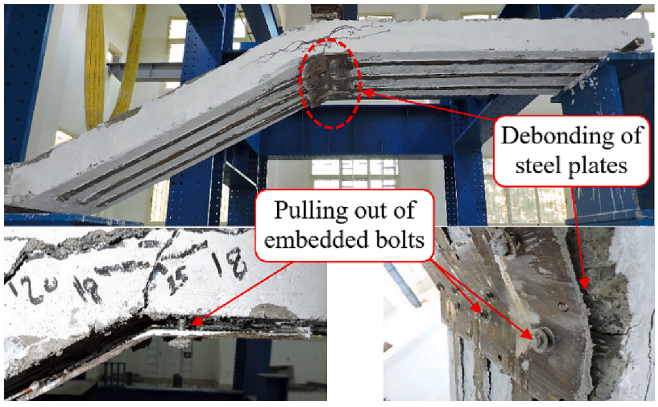

Fig. 11. Crack patterns of slab S-E-CSPs.

reduced the number of cracks in comparison with the control slab S-S0. Moreover, these cracks were remarkably concentrated closed to the critical zone in the bend under opening moments. Under higher loads, some longitudinal hair cracks developed just beside steel plates as shown in Fig. 10(b). Just before failure, the transverse steel plates started to deform associated with pulling out of emended bolts. Finally, the tested stair slab failed by the flexural-compression failure mode accompanied with pull-out of embedded bolts as shown in Fig. 10(a). The recorded ultimate loads of slabs S-E-LSPs and S-E-CSPs were 39.94kN and 42.85kN, respectively. This indicates that the applications of steel plates improved the ultimate load by about 53–64%.

Group G2 was exploited to evaluate the effectiveness of NSMSB strengthening technique through three tested slabs: S-N-10D, S-N-15D, and S-N-20D. The crack patterns of this group are shown in Figs. 12 to 14. Generally, the first crack was detected at the bottom line of the bend under opening moments at load values ranged from 9 kN to 11.5kN (about 33% and 39% of P_u) as remarked in Figs. 12 to 14. Compared to the cracking load of the control slab, the method of strengthening improved the cracking loads of S-N-10D, S-N-15D, and S-N-20D by about 57%, 80%, and 100%, respectively. It is seen from Table 3 that the longer the embedded length (l_d), the higher the cracking load. As the load was increased, some flexural cracks developed along the slab axis and eventually extended to the top surface. In addition, these cracks started to propagate at the mid-span of the bottom surface of the bend subjected to opening moments. Moreover, the first crack formed at the bottom of the bend under opening moments become wider. As a result, the whole stair slab was broken into horizontal and inclined parts as shown in Fig. 12. These cracks were marked at loads within range of about 53% to 57% of P_u. The major crack continued to propagate until the slab failed. The main failure modes of the stair slabs strengthened by NSMSB were flexural cracking and pull-out of steel bars as can be seen in Fig. 12(b). The recorded ultimate loads (P_{us}) were 26.74kN, 28.08kN, and 29.52kN for slabs S-N-10D, S-N-15D, and S-N-20D, respectively.

3.2. Ultimate loads

Table 4 compares the P_u values of the tested stair slabs obtained from experiments. The application of EBSP in the tested stair slabs S-E-LSPs

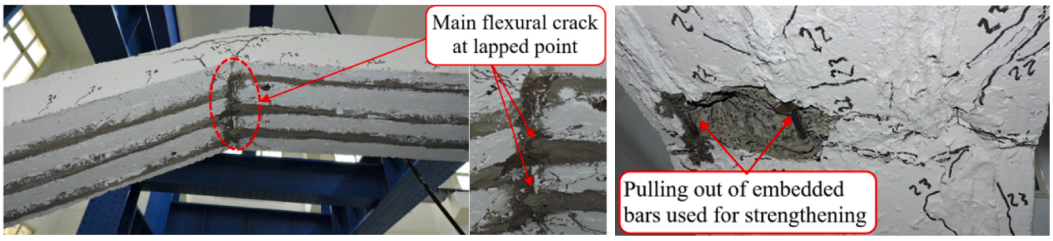

Fig. 12. Crack patterns of slab S-N-10D: (a) main flexural cracks; (b) pulling out of embedded bars used for strengthening.

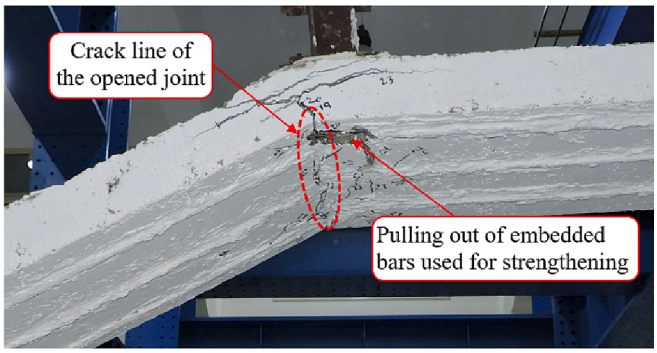

Fig. 13. Crack patterns of slab S-N-15D.

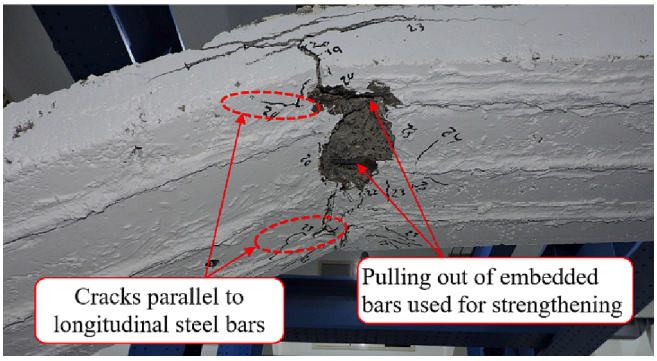

Fig. 14. Crack patterns of slab S-N-20D.

and S-E-CSPs in Group G1 resulted in an enhancement of P_u by about 53% and 64%, respectively. On the other hand, although NSMSB system used in Group G2 presented a satisfied performance at the cracking stage, it did not achieve a higher increase in P_u, only 13% for $Le = 20D$. This may be attributed to the earlier pull-out failure of longitudinal bars. However, the bonding between steel plates and concrete due to adhesive chemical epoxy and bolts prevented the earlier pull-out failure, thereby increasing the load-carrying capacity of the stair slabs. Generally, it may be observed that steel plates with thickness not less than 4 mm should be used to strengthen stair slabs.

3.3. Load-displacement response and elastic index

The measured load–deflection curves of tested stair slabs are depicted in Fig. 15. Table 4 provides the vertical deflection values corresponding to the cracking and ultimate loads (Δ_{cr}) and (Δ_{Pu}), respectively. The elastic stiffness indies (K) evaluated as the slope of the linear elastic part of the load–deflection curves for the tested stair slabs are summarized in Table 4.

Generally, all tested stair slabs exhibited linear behavior up to the load which was very close to the cracking load. Such linear performance approximately met with the beginning of loading up to the appearance of first crack. After concrete cracking, all strengthened stair slabs entered the non-linear regime with hardening behavior up to the ultimate load; a small increase in load led to a large increase in deflection. Beyond that, the softening appeared up to failure; little diminishing in load resulted in remarkable increase in deflection up to failure. the linear, hardening, and softening behaviors are illustrated in Fig. 15.

It appears from Figs. 15-16 that the tested stair slabs strengthened by EBSP carried higher ultimate loads than those strengthened by NSMSB. In addition, the strengthening technique using EBSP improved the K-values of the stair slabs by about 1.96 to 2.96 times that of S-S0 as given in Table 4.

The strengthening method using NSMSB considerably improved the behavior of stair slabs as demonstrated in Fig. 15(b). However, the load-carrying capacity and the displacement ductility of the stair slabs could be impacted by the embedded length (L_e) of the steel bars. In addition, the use of NSMSB to strengthen stair slabs resulted in a good contribution to the elastic K-value as shown in Table 4. This enhancement was estimated by about 1.6–2.56 times that of the control slab. It is suggested that the embedded length of steel bars should be greater than 10D.

Table 4
Test Results.

Gro.	Specimen ID	Cracking Stage				Ultimate Stage			Elastic Stiffness Index (K)	K_S/K_0	Absorbed Energy (E)	Mode of Failure
		P_{cr} (kN)	P_{crS}/P_{crS0}	Δ_{cr} (mm)	W_{cr} (mm)	P_u (kN)	P_{uS}/P_{uS0}	Δ_{Pu} (mm)				
G1	S-S0	5.7	1.00	0.33	0.23	26.0	1.00	6.72	17.2	1.00	411.17	F + P_{MS}
	S-E-LSPs	13.5	2.36	0.4	0.19	39.94	1.53	11.60	33.75	1.96	1028.83	F + P_B
	S-E-CPs	15.3	2.68	0.30	0.16	42.85	1.64	14.60	51.0	2.96	1292.62	F + P_B
G2	S-S0	5.7	1.00	0.33	0.23	26.0	1.00	6.72	17.2	1.00	411.17	F + P_{MS}
	S-N-10D	9.0	1.57	0.31	0.24	26.74	1.02	10.31	29.03	1.68	613.71	F + P_{SS}
	S-N-15D	10.3	1.80	0.28	0.21	28.08	1.08	16.36	36.7	2.13	728.18	F + P_{SS}
	S-N-20D	11.5	2.01	0.26	0.18	29.52	1.13	11.08	44.2	2.56	749.12	F + P_{SS}

P_{cr}: First cracking load; **Δ_{cr}:** Deflection recorded at P_{cr}; **W_{cr}:** Crack width recorded at P_{cr}; **P_U:** Ultimate load; **Δ_{PU}:** Deflection recorded at P_u; **K:** elastic index; **E:** Absorbed energy; **F:** Flexural failure; **P_{MS}:** Pulling-out of main steel bars; **P_B:** Pulling-out of embedded bolts; and **P_{SS}:** Pulling-out of flexural steel bars used for strengthening.

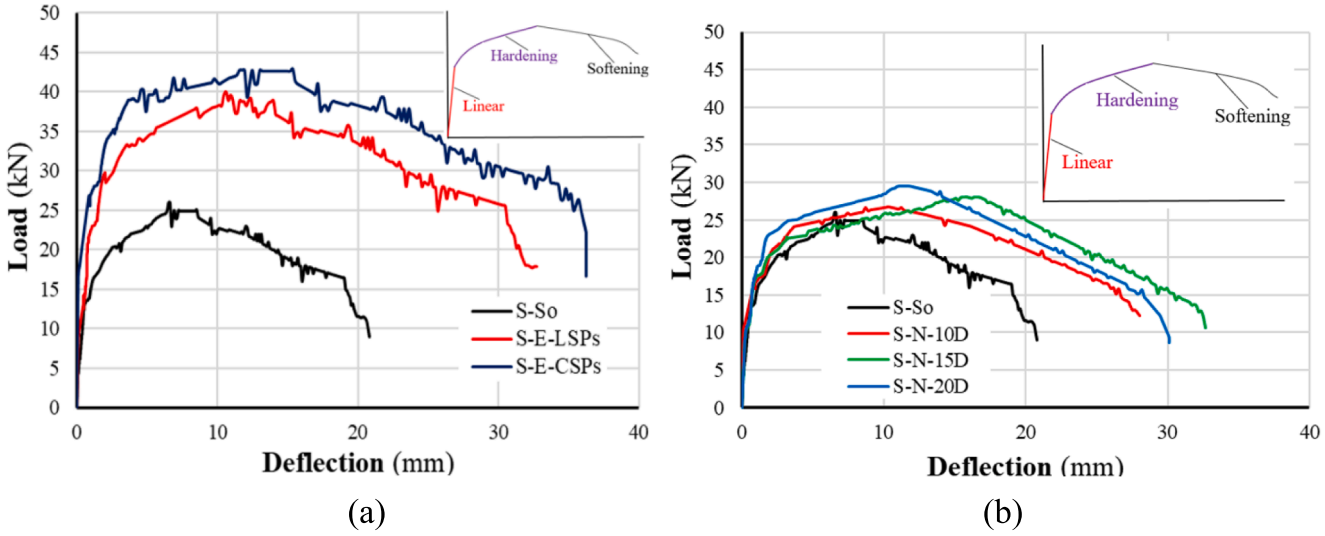

Fig. 15. Load-deflection curves: (a) Group G1; (b) Group G2.

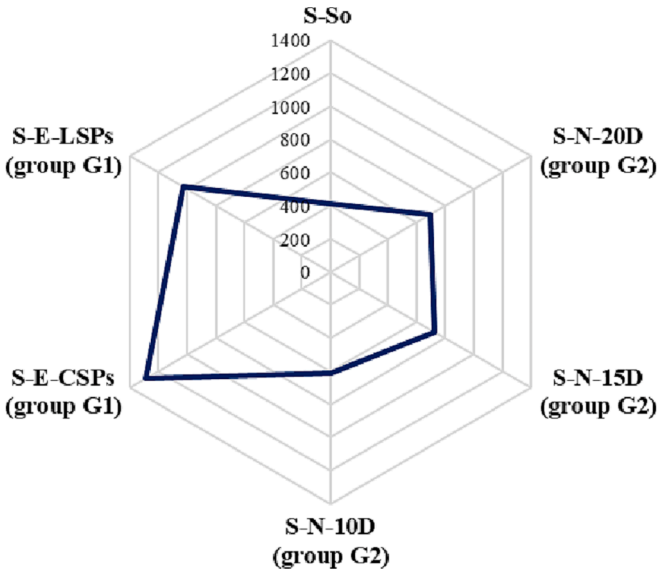

Fig. 16. The absorbed energy (*E*) values for all slabs (kN.mm).

3.4. Absorbed energy

Table 4 presents the values of absorbed energy (E) evaluated for the tested slabs as the integration of the total area under the load–deflection curve up to failure. It was founded that the use of EBSP led to a remarkable increase in the energy absorption capacity. It can be seen from Table 4 that the *E* values of S-E-LSPs and S-E-CSPs strengthened by EBSP were about 150% and 214% higher than that of the control slab, respectively. As shown in Fig. 15, the *E* values of stair slabs strengthened by NSMSB increased about 49%, 77%, and 82% for the embedded lengths (L_e) of 10D, 15D, and 20D, respectively. It should be mentioned that although the NSMSB technique offers lesser strength improvement than the EBSB method, it has been widely used due to the quick and easy installation and low costs.

4. Numerical simulation

4.1. Constitutive modeling of materials and sensitivity analysis

The commercial software ABAQUS was employed to simulate the responses of tested stair slabs. The Concrete Damage Plasticity (CDP) model available in ABAQUS was adopted in the present study to model the plastic behavior of concrete due to its ability to define damage generated from cracking and nonlinear deformation of concrete in compression and tension [32–38]. Plastic damage models developed by Lubliner et al. [39] have been commonly used to estimate the yield surface hardening parameters of traditional concrete. The results obtained from both tension and compression tests were employed to calibrate concrete material stress–strain behavior to identify the most suitable parameters. The stress–strain relationship developed by Carreira and Chu [42] was employed to model the concrete in compression. A linear relationship was assumed for concrete in tension before and after cracking [40–43]. Fig. 4 provides the stress–strain law of NC under tensile and compressive stresses for numerical modeling.

Several attempts were made to determine the most suitable values of the constitutive parameters used in CDP model for normal concrete. These parameters were viscosity relaxation parameter (μ), angle of dilation (ψ), eccentricity (e), ratio of second stress invariant on the tensile to compressive meridian (K_c), and ratio of biaxial to uniaxial compressive yield stresses (f_{bo}/f_{co}).

Analyses were conducted with different μ values changed from 0.00 to 1.00×10^{-8}, 1.00×10^{-7}, 1.00×10^{-6}, 1.00×10^{-5}, 1.00×10^{-4}, and 0.001. However, previous studies [33,44,45] recommended that the zero-value is an acceptable outcome compared to the very stiff run with higher μ as previously reported [53]. It was found that the suitable angle of dilation (ψ) is 35° as recommended by researchers [40,41]. The K_c value is generally between 0.64 and 0.80 as previously mentioned [40,46 to 52]; however; the sensitivity analysis confirmed the defaulted value of 0.66 in ABAQUS [33]. The f_{bo}/f_{co} ratio ranged from 1.10 to 1.16 with respect to previous studies [51,52]; however, the 1.16 value was credited in the current investigation. The present model adopted the defaulted value of $e = 0.1$ recommended by software program.

Two different steel bars were defined in this study: 10 mm and 12 mm diameter of deformed steel bars with same material characteristics as shown in Fig. 4(a). To create a finite element model with less computational cost, the measured stress–strain curve was idealized as a piecewise linear one as shown in Fig. 4.

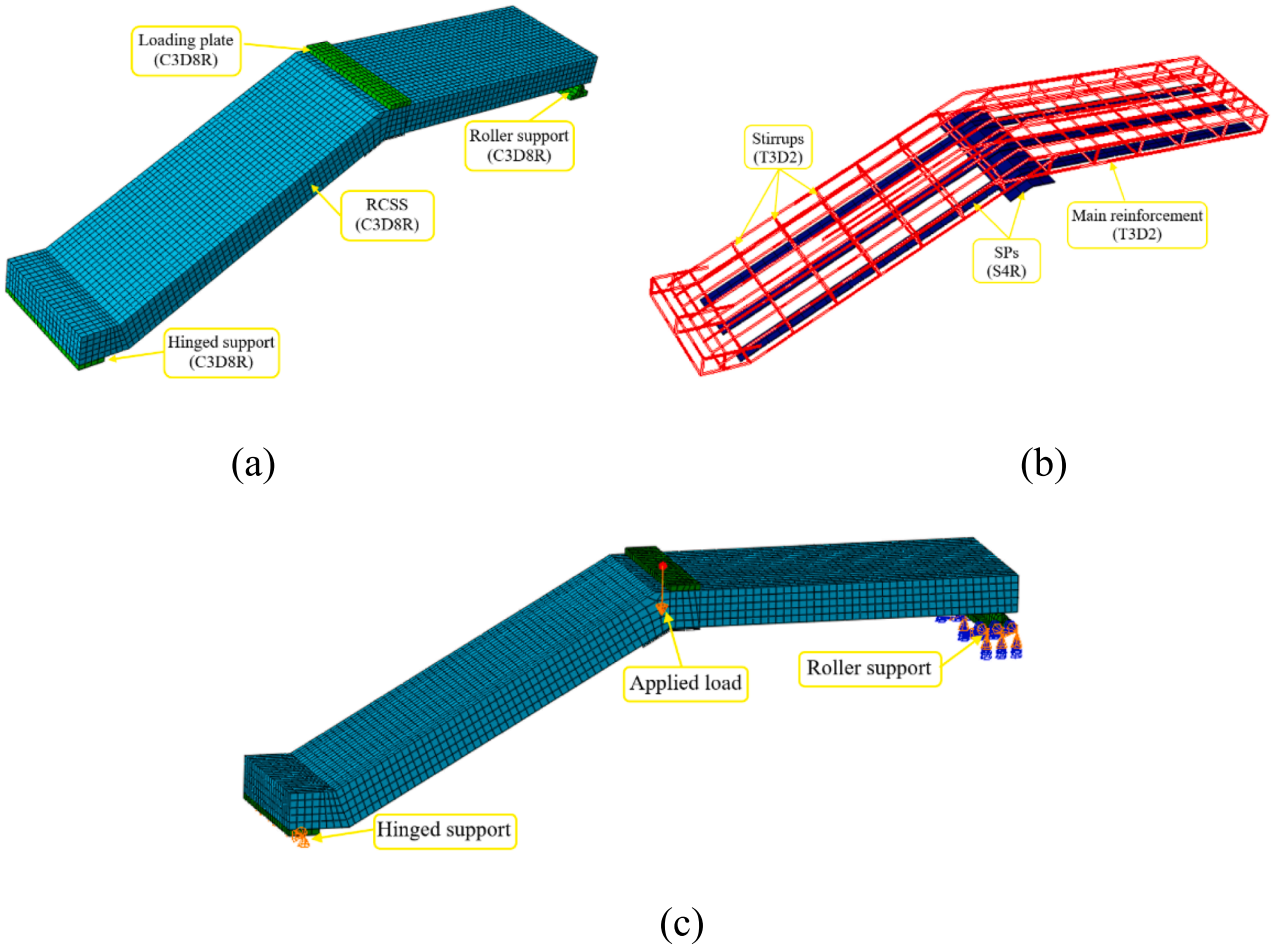

Fig. 17. Finite element model: (a) concrete elements; (b) steel elements; (c) loading and boundary conditions.

4.2. Development of finite element model

A nonlinear three-dimensional Finite Element (FE) model was created to model the responses of strengthened RCSS in Group G1 subjected to static monotonic loading up to collapse. The continuum, three-dimensional and eight-node linear hexahedral solid element with reduced integration (C3D8R) available in ABAQUS was employed to mesh the RC stair slab and thick steel plates as shown in Fig. 17(a). The two-node and linear truss element namely T3D2 was utilized to model the steel bars as depicted in Fig. 17(b). The four-node shell element with reduced integration (S4R) was employed to represent thin steel plates as shown in Fig. 17(b). The three-dimensional element C3D8R was employed to mesh the thick loading plate with larger stiffness. The boundary condition of the stair slab was modeled as simply supported. The loading and boundary condition of the FE model are shown in Fig. 17(c). The developed model with about 24-mm meshing size provided a satisfied performance with less computational cost. The mesh of the developed FE model can be seen in Fig. 17.

The interaction between concrete and steel bars was assumed to be perfect bond which is available in ABAQUS under embedded element mechanism. This assumption was considered by employing the concrete slab as the host region while the steel bar truss elements were chosen as the embedded ones. The bond between the thick plates and concrete slab was modeled as perfect. The concrete surface of the stair slab was set as the master while the surfaces of steel plates were treated as slave ones. In order to model the contact between SPs and lower side of RCSS, the tie-surface to surface constrain was assumed herein. This assumption was achieved by employing the upper surface of SPs to be the slave while the other opposite of slab surface was set to be the master one as previously reported [45].

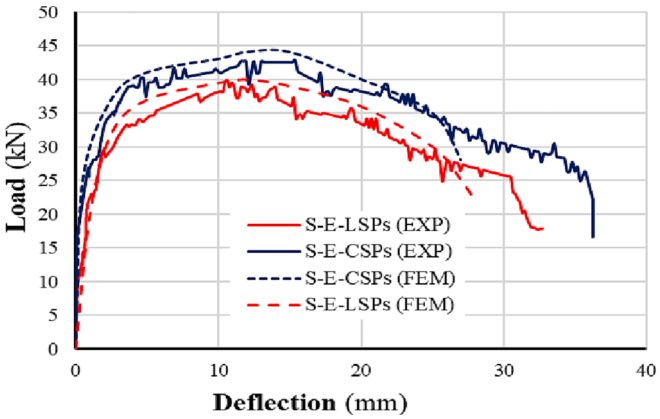

Fig. 18. Load-displacement responses of G1 specimens obtained experimentally and numerically.

4.3. Verification

The accuracy of the developed FE model has been established by comparing the numerical simulations with experimentally measured data in terms of load–deflection response, failure mode, cracking and ultimate load values. The load–displacement responses obtained numerically are compared with experimental counterparts in Fig. 18.

Table 5
Comparison between numerical and experimental results.

Specimen ID	P_{cr} (kN)			Δ_{cr} (mm)			P_u (kN)			Δ_{Pu} (mm)		
	EX	FE	FE/EX	EX	FE	FE/EX	EX	FE	FE/EX	EX	FE	FE/EX
S-E-LSPs	13.5	14.3	1.059	0.4	0.43	1.075	39.94	41.02	1.027	11.60	12.3	1.060
S-E-LSPs	15.3	16.6	1.084	0.30	0.32	1.066	42.85	43.95	1.025	14.60	15.25	1.044
Avg			1.071			1.070			1.026			1.052
SD			0.0176			0.0063			0.0014			0.0113
COV			0.0164			0.0058			0.0013			0.0107

Ex: Experimental; **FE**: Finite Element Model; **Avg:** Average; **SD:** Standard deviation; **COV:** Coefficient of variation.

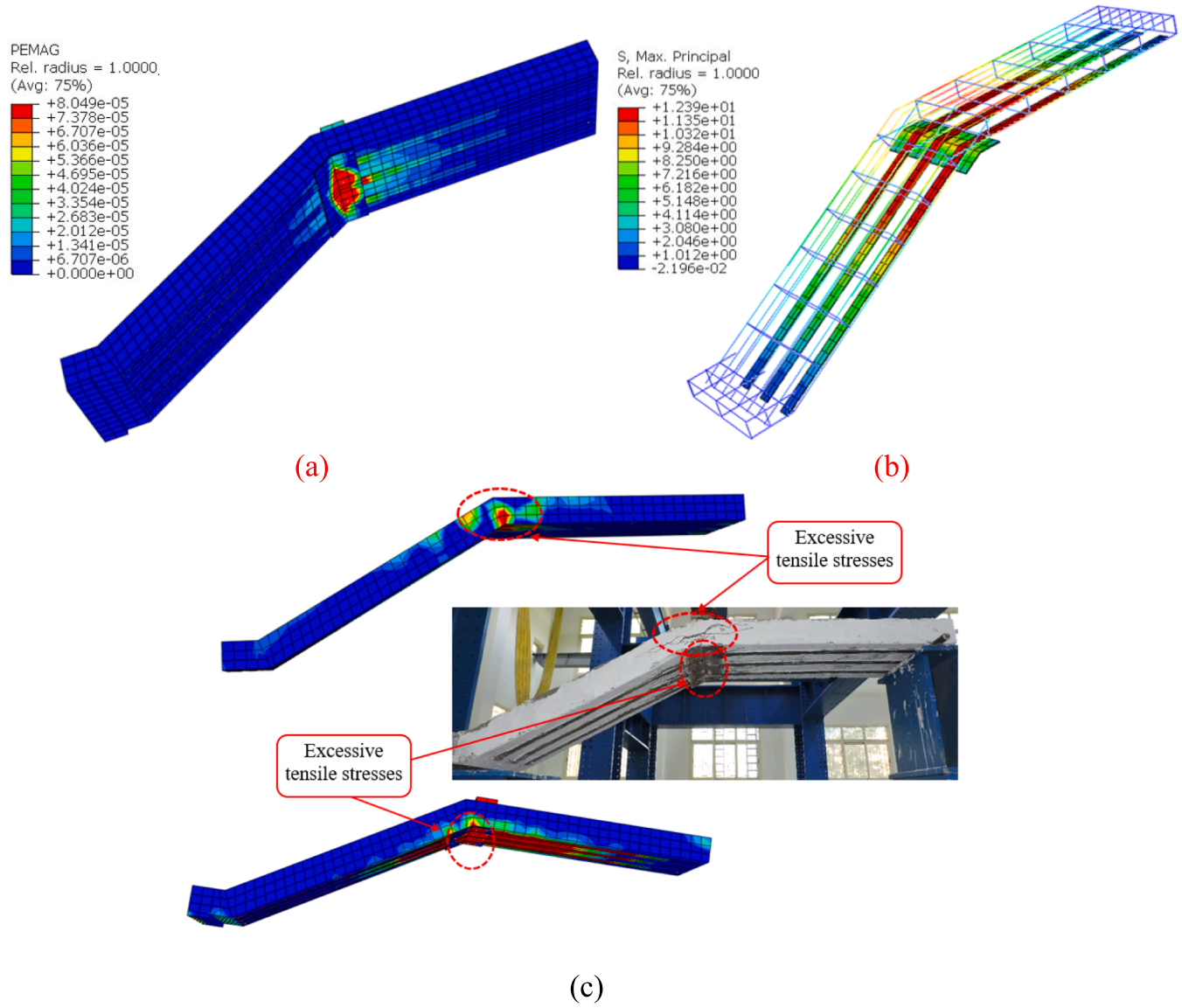

Fig. 19. Predicted cracking pattern: (a) cracking pattern; (b) stress contours for steel elements; (c) verification of cracking pattern.

Both experimental and numerical ultimate loads (P_{us}) together with their corresponding deflections are provided in Table 5. The main failure modes predicted by the FE model can be seen in Fig. 19.

The load–displacement responses obtained numerically are compared with experimental counterparts in Fig. 18. It can be observed from Fig. 18 that the FE model simulates well the experimentally measured load–deflection curves of stair slabs. As shown in Table 4, the cracking and ultimate loads of the tested slabs are accurately predicted by the FE model. The average value of $P_{cr\ FE}/P_{cr\ EXP}$ ratios is 1.071 with standard deviation (SD) of 0.0176. The average values of $P_{U\ FE}/P_{U\ EXP}$ is 1.026 with SD of 0.0014. The mean value of $\Delta_{Pu\ FE}$ / $\Delta_{Pu\ EXP}$ is 1.052 with SD of 0.0113. The predicted failure mode is compared with test results in Fig. 18. It should be noted that the model validation may be captured by the softening behavior manifested in load–deflection response shown in Fig. 18. This may be attributed to the deterioration occurred in concrete part followed by an obvious contribution arising from steel plates. Also, this figure shows that the FE model generally captures well the failure pattern of the tested stair slab. The FE model

indicates that the major crack initiated at bottom of the bend under opening moments and extended to the top surface as observed in the test. Moreover, numerical simulation shows that high tensile stresses developed in the longitudinal steel plates within the mid zone as shown in Fig. 19(b). This may lead to the better understanding of the remarkable deformation occurred experimentally at such steel plates as shown in Fig. 19(c).

5. Conclusions

This paper has reported the experiments on the performance of full-scale reinforced concrete stair slabs that were strengthened with externally bonded steel plates and near surface mounted steel bars. The impacts of the strengthening techniques, type and configuration of reinforcement used for strengthening on the responses of such slabs have been investigated and examined. A nonlinear finite element model of strengthened stair slabs has been developed by means of utilizing ABAQUS and verified by experimental data.

Based on the experimental and numerical studies, the following conclusions are drawn:

- The application of EBSP, with thickness of 4 mm, could significantly alter the mode of failure and cracking characteristics of stair slabs. The cracking loads of stair slabs strengthened by EBSP were about 136% to 168% higher than that of the one without strengthening; their ultimate loads were improved by about 53% to 64%, respectively.
- The NSMSB strengthening system considerably improved the elastic behavior and cracking loads of stair slabs. Using the embedded lengths of L_e = 10D, 15D and 25D enhanced the cracking load by about 57%, 80%, and 101%, respectively; it enhanced the K-values by about 1.68 to 2.13 and 2.56 times that of the control slab, respectively.
- The EBSP significantly increased the absorbed energies (E) of slabs S-E-LSPs and S-E-CPs by about 2.50 and 3.14, respectively, compared to the control slab.
- The developed FE model predicts well the structural performance of strengthened and non-strengthened stair slabs with a high degree of accuracy. Therefore, the FE model can be employed to exploit parametric analysis in the future.

CRediT authorship contribution statement

Ahmed A. Hamoda: Conceptualization, Methodology, Software, Validation, Formal analysis, Investigation, Data curation, Writing – original draft, Visualization, Project administration. **Boshra A. Eltaly:** Formal analysis, Investigation, Data curation, Writing – review & editing. **Rania E. Sera:** Software, Validation, Formal analysis, Investigation, Writing – review & editing. **Qing Quan Liang:** Visualization, Writing – review & editing.

Declaration of Competing Interest

The authors declare that they have no known competing financial interests or personal relationships that could have appeared to influence the work reported in this paper.

Data availability

Data will be made available on request.

References

[1] Sahranavard S, Jahangir H, Kazemi HH. An experimental and numerical investigation of RC slabs externally strengthened by perforated steel plates. Structures 2022;45:1239–52.

[2] Wang Z, Wang M, Xu Q, Harries KA, Li X, Gao R. Experimental research on prestressed concrete hollow-core slabs strengthened with externally bonded bamboo laminates. Eng Struct 2021;244:112786.

[3] Kadhim MMA, Jawdhari A, Adheem AH, Fam A. Analysis and design of two-way slabs strengthened in flexure with FRCM. Eng Struct 2022;256:113983.

[4] Daneshvar K, Moradi MJ, Ahmadi K, Hajiloo H. Strengthening of corroded reinforced concrete slabs under multi-impact loading: Experimental results and numerical analysis. Constr Build Mater 2021;284:122650.

[5] Muciaccia G, Khorasani M, Mostofinejad D. Effect of different parameters on the performance of FRP anchors in combination with EBR-FRP strengthening systems: A review. Constr Build Mater 2022;354:129181.

[6] Azevedo AS, Firmo JP, Correia JR, Chastre C, Biscaia H, Franco N. Fire behaviour of CFRP-strengthened RC slabs using different techniques–EBR, NSM and CREatE. Compos B Eng 2022;230:109471.

[7] Sabzi J, Esfahani MR, Ozbakkaloglu T, Farahi B. Effect of concrete strength and longitudinal reinforcement arrangement on the performance of reinforced concrete beams strengthened using EBR and EBROG methods. Eng Struct 2020;205:110072.

[8] Afefy HM, Kassem NM, Mahmoud MH, Taher SEDF. Efficient strengthening of opened-joint for reinforced concrete broken slabs. Compos Struct 2016;136:602–15.

[9] Dong Z, Deng M, Dai J, Song S. Flexural strengthening of RC slabs using textile reinforced mortar improved with short PVA fibers. Constr Build Mater 2021;304:124613.

[10] Wang Z, Liang X, Wang Y, Zhai T. Experimental and theoretical investigations on the flexural behavior of RC slabs with steel-PVA hybrid fiber reinforced cementitious composite (HFRCC) permanent formwork. Case Stud Constr Mater 2022;17:e01432.

[11] Zhang HY, Liu HY, Kodur V, Li MY, Zhou Y. Flexural behavior of concrete slabs strengthened with textile reinforced geopolymer mortar. Compos Struct 2022;284:115220.

[12] Hassan T, Rizkalla S. Bond mechanism of NSM FRP bars for flexural strengthening of concrete structures. ACI Struct J 2004;101(6):830–9.

[13] Kotynia, R. Analysis of the flexural response of NSM FRP-strengthened concrete beams. In Proceedings of the 8th International Symposium on Fiber Reinforced Polymer Reinforcement for Reinforced Concrete Structures (FRPRCS-8), 2007; July, pp. 16-18.

[14] Soliman SM, El-Salakawy E, Benmokrane B. Flexural behaviour of concrete beams strengthened with near surface mounted FRP bars. In: Proc. on CDROM, 4th int. conf. on FRP composites in civil engineering (CICE2008), Zurich, Switzerland; 22–24 July, 2008.

[15] Soliman SM, El-Salakawy E, Benmokrane B. Flexural behaviour of concrete beams strengthened with near surface mounted fibre reinforced polymer bars. Can J Civ Eng 2010;37(10):1371–82.

[16] Lee D, Cheng L, Yan-Gee Hui J. Bond characteristics of various NSM FRP reinforcements in concrete. J Compos Constr 2012;17(1):117–29.

[17] Hollaway, L. C. Fibre-reinforced polymer (FRP) composites used in rehabilitation. In *Strengthening and rehabilitation of civil infrastructures using fibre-reinforced polymer (FRP) composites* 2008; pp. 45-82, Woodhead Publishing.

[18] Mohammadi M, Mostofinejad D, Barghian M. Effects of surface preparation method on FRP-concrete bond strength under alkaline conditions. J Compos Constr 2017;21(4):04017010.

[19] Kamonna HH, Abd Al-Sada DJ. Strengthening of one-way reinforced concrete slabs using near surface mounted bars. Mater Today: Proc 2021;42:1843–53.

[20] Rahal KN, Rumaih HA. Tests on reinforced concrete beams strengthened in shear using near surface mounted CFRP and steel bars. Eng Struct 2011;33(1):53–62.

[21] Saadah M, Ashteyat A, Murad Y. Shear strengthening of RC beams using side near surface mounted CFRP ropes and strips. Structures 2021;32:380–90.

[22] Abdallah M, Al Mahmoud F, Boissière R, Khelil A, Mercier J. Experimental study on strengthening of RC beams with Side Near Surface Mounted technique-CFRP bars. Compos Struct 2020;234:111716.

[23] Almusallam TH, Elsanadedy HM, Al-Salloum YA, Alsayed SH. Experimental and numerical investigation for the flexural strengthening of RC beams using near-surface mounted steel or GFRP bars. Constr Build Mater 2013;40:145–61.

[24] Krzywoń R. Behavior of EBR FRP strengthened beams exposed to elevated temperature. Procedia Eng 2017;193:297–304.

[25] Mostofinejad D, Kashani AT. Experimental study on effect of EBR and EBROG methods on debonding of FRP sheets used for shear strengthening of RC beams. Compos B Eng 2013;45(1):1704–13.

[26] del Rey Castillo E, Dizhur D, Griffith M, Ingham J. Strengthening RC structures using FRP spike anchors in combination with EBR systems. Compos Struct 2019;209:668–85.

[27] Bakis CE, Bank LC, Brown VL, Cosenza E, Davalos JF, Lesko JJ, et al. Fiber-reinforced polymer composites for construction-state-of-the-art review. J Compos Constr 2002;6(2):73–87.

[28] Mazaheripour H, Ghanbarpour S, Mirmoradi SH, Hosseinpour I. The effect of polypropylene fibers on the properties of fresh and hardened lightweight self-compacting concrete. Constr Build Mater 2011;25(1):351–8.

[29] American Concrete Institute. Committee 440. Guide for the Design and Construction of Externally Bonded FRP Systems for Strengthening Concrete Structures: ACI 440.2 R-08, 2008, American Concrete Institute.

[30] Al-Rousan RZ, Alkhawaldeh A. Numerical simulation of the influence of bond strength degradation on the behavior of reinforced concrete beam-column joints externally strengthened with FRP sheets. Case Stud Constr Mater 2021;2021(15):e00567.

[31] ACI Committee 318. Building code requirements for structural concrete (ACI 318-08) and commentary. American Concrete Institute; 2014.

[32] Hamoda A, Hossain KMA. Numerical assessment of slab–column connection additionally reinforced with steel and CFRP bars. Arab J Sci Eng 2019;44(10):8181–204.
[33] Carreira DJ, Chu KH. Stress-strain relationship for plain concrete in compression. Journal Proceedings 1985;82(6):797–804.
[34] Nataraja MC, Dhang N, Gupta AP. Stress–strain curves for steel-fiber reinforced concrete under compression. Cem Concr Compos 1999;21(5–6):383–90.
[35] El-Mandouh MA, Elsamak G, O. Rageh B, Hamoda A, Abdelazeem F. Experimental and numerical investigation of one-way reinforced concrete slabs using various strengthening systems. Case Stud Constr Mater 2023;18:e01691.
[36] Hamoda A, Elsamak G, Emara M, Ahmed M, Liang QQ. Experimental and numerical studies of reinforced concrete beam-to-steel column composite joints subjected to torsional moment. Eng Struct 2023;275:115219.
[37] Barros JA, Lourenço LA, Soltanzadeh F, Taheri M. Retracted article: Steel fibre reinforced concrete for elements failing in bending and in shear. Eur J Environm Civil Eng 2014;18(1):33–65.
[38] Hamoda A, Emara M, Mansour W. Behavior of steel I-beam embedded in normal and steel fiber reinforced concrete incorporating demountable bolted connectors. Compos B Eng 2019;174:106996.
[39] Lubliner J, Oliver J, Oller S, Oñate E. A plastic-damage model for concrete. Int J Solids Struct 1989;25(3):299–326.
[40] Hamoda A, Emara M, Abdelazeem F, Ahmed M. Experimental and numerical analysis of RC beams strengthened with ECC and stainless steel strips. Mag Concr Res 2023;75(5):251–70.
[41] Jahani Y, Baena M, Barris C, Torres L, Sena-Cruz J. Effect of fatigue loading on flexural performance of NSM CFRP-strengthened RC beams under different service temperatures. Eng Struct 2022;273:115119.
[42] Ahmed M, Sheikh MN, Hadi MNS, Liang QQ. Numerical modeling of self-compacting concrete columns longitudinally reinforced with steel tubes under axial loading. Eng Struct 2022;270:114913.
[43] Abrishambaf A, Barros JA, Cunha VM. Tensile stress–crack width law for steel fibre reinforced self-compacting concrete obtained from indirect (splitting) tensile tests. Cem Concr Compos 2015;57:153–65.
[44] Elsamak G, Salama MI, Hamoda A. Behavior of Precast Segmental Beams Made of High-strength Concrete and Ultra-high Performance Fiber Concrete Connected by Shear Keys Technique. Arab J Sci Eng 2023;48(4):4907–23.
[45] Hamoda A, Ahmed M, Sennah K. Experimental and numerical investigations of the effectiveness of engineered cementitious composites and stainless steel plates in shear strengthening of reinforced concrete beams. Struct Concr 2023;24(2):2778–99.
[46] Lee J, Fenves GL. Plastic-damage model for cyclic loading of concrete structures. J Eng Mech ASCE 1998;124(8):892–900.
[47] Ci J, Kong L, Ahmed M, Liang QQ, Hamoda A, Chen S, et al. Experimental and numerical studies of axially loaded square concrete-encased concrete-filled large-diameter steel tubular short columns. Struct Concr 2022;23(5):2748–69.
[48] Ahmed M, Liang QQ, Hamoda A. Fiber element modeling of circular double-skin concrete-filled stainless-carbon steel tubular columns under axial load and bending. Adv Struct Eng 2022;25(5):1114–35.
[49] Hamoda A, Basha A, Fayed S, Sennah K. Experimental and numerical assessment of reinforced concrete beams with disturbed depth. Int J Concr Struct Mater 2019;13(1):1–28.
[50] Ci J, Ahmed M, Liang QQ, Chen S, Chen W, Sennah K, et al. Experimental and numerical investigations into the behavior of circular concrete-filled double steel tubular slender columns. Eng Struct 2022;267:114644.
[51] Le, T. T., Patel, V. I., Liang, Q. Q., Huynh, P., & Ha, N. S. (2022). Numerical analysis of square concrete-filled double-skin tubular columns with outer stainless-steel tube. Structural Concrete 2022; 23(5):2968-2985.
[52] Yu K, Wang Y, Yu J, Xu S. A strain-hardening cementitious composites with the tensile capacity up to 8%. Constr Build Mater 2017;137:410–9.
[53] Yuan F, Wei W, Hu R. Shear strengthening of reinforced concrete beams with high-strength steel wire and engineered cementitious composites. Adv Struct Eng 2022;25(1):158–70.
[54] Naser MZ, Hawileh RA, Abdalla JA. Fiber-reinforced polymer composites in strengthening reinforced concrete structures: A critical review. Eng Struct 2019;2019(198):109542.
[55] Khalifa, A., & Nanni, A. (2002). Rehabilitation of rectangular simply supported RC beams with shear deficiencies using CFRP composites. Construction and building materials 2002; 16(3):135-146.
[56] Hollaway LC. A review of the present and future utilisation of FRP composites in the civil infrastructure with reference to their important in-service properties. Constr Build Mater 2010;24(12):2419–45.
[57] Agarwal A, Nanda B, Maity D. Experimental investigation on chemically treated bamboo reinforced concrete beams and columns. Constr Build Mater 2014;71:610–7.